Winter phytoplankton bloom induced by subsurface upwelling and entrainment southwest of Luzon Strait

JiuJuan Wang[1, 2], DanLing Tang[1, 2, *]

1. Research Center of Remote Sensing and Marine Ecology Environment (RSMEE), LED, South China Sea Institute of Oceanology, Chinese Academy of Sciences, 164 West Xingang Road, Guangzhou, 510301, PR China

2. Graduate University of Chinese Academy of Sciences, Beijing 100049, PR China

Corresponding author: Tel. /fax: +86 20 89023203.E-mail addresses: lingzistdl@126.com (D.L. Tang); http://lingzis.51.net/index.html

Abstracts

Phytoplankton blooms are appearing in winter (Nov.-Feb.) in the southwest of Luzon Strait , South China Sea , which is an oligotrophic region in general. To understand the mechanism of the winter bloom dynamics, this study analyzes multiyear (2000-2007) remote sensing data, ecological sampling data and physical oceanographic parameters. The Empirical Orthogonal Function analysis confirms a high occurrence area about 2.58×10^4 km^2 of winter phytoplankton blooms in the southwest of Luzon Strait. Moreover, a cold temperature core (< 19.0 ℃) with low dissolved oxygen concentration (< 4.55 mg L^{-1}) is observed at the depth of 50 m, and the concentrations of Nitrate, Phosphorus, and Silicon display a narrow fluctuation in the top 50 m and increased rapidly below the 50 m depth. The local mixed-layer depth reaches to its deepest (> 60 m) with strongest northeast wind (>10 m s^{-1}) during the bloom period. The results demonstrate that southwest of Luzon Strait experiences a repeated winter phytoplankton bloom controlled by adequate nutrients under the combinated action of subsurface upwelling (observed at about 50 m under sea surface) and upper mixed-layer entrainment. Wind-related physical processes of offshore Ekman transport and turbulent mixing play an important role in regulating the biological dynamics.

Keywords: winter phytoplankton bloom; subsurface upwelling; mixed-layer depth; wind; Luzon Strait

1. Introduction

The South China Sea (SCS) is the largest marginal sea in the western tropical Pacific. Most oceanographic studies of the SCS are related to Luzon Strait which connects the Western Pacific Ocean to the SCS (Fig.1A), including Kuroshio intrusion (Farris and Wimbush, 1996), mesoscale eddies (Wu and Chiang, 2007), internal waves (Liu and Hsu, 2003). The hydrological characteristics of Luzon Strait are complex and are influenced by the general conditions of the SCS, which belong to the Asian monsoon system and neighbor with four monsoon subsystems: the subtropical East Asian monsoon, the tropical Indian monsoon, the Western North Pacific monsoon, and the Australian monsoon (Wang et al., 2009). Northeast monsoon winds over the SCS blow in winter time at stronger mean speed of 9 m s^{-1} compared with summer winds; southwest monsoon winds with the average wind speed of 6 m s^{-1} prevail during summer period (Wyrtki, 1961).

Though the SCS is a relatively oligoltrophic tropical-subtropical ocean (Tang et al., 2004b; Tang et al., 1999), ecological implications at the vicinity of Luzon Strait are evidenced in terms of winter phytoplankton blooms in certain years (Chen et al., 2006; Peñaflor et al., 2007; Tang et al., 1999). Tang (1999) first reported this phenomenon appeared in winters of 1981, 1982 and 1984 with the limited remote sensing Coastal Zone Color Scan (CZCS) data in last century. Using Moderate Resolution Imaging Spectroradiometer (MODIS)-derived data, Peñaflor (2007) indecated that southwest of Luzon Strait experienced blooms in 2003 and 2004 wintertime. The winter bloom was also detected in 1999 by in *situ* study (Chen et al., 2006). Hydrological conditions around Luzon Strait were complex and the related environmental variability may have some influences on the biological processes, however,

previous reports have been constrained by short-term time studies, which were only able to reflect about the relationship between the blooms in the specific year with particular environmental situation. Field survey data of temperature, salinity and dissolved oxygen concentration identified a winter upwelling region southwest of Luzon Strait (Shaw et al., 1996). Shaw (1996) pointed out that the offshore upwelling in this area was contributed to a remotely forced component arising from the basin-wide gyre circulation. Using numerical modeling, Chao et al (1996) noted that the upwelling was associated with inflow of Pacific water during winter. Qu (2000) argued that wind stress curl or direct Ekman pumping might play a major role in generating the winter upwelling off Luzon Strait from computing the wind stress curl and its seasonal variability. In the point of previous studies, upwelling might be responsible for the winter phytoplankton blooms southwest of Luzon Strait (Peñaflor et al., 2007; Tang et al., 1999). But the existence of the winter upwelling or the mechanism of this upwelling is still without a definite answer, so the winter bloom dynamics near Luzon Strait and the state of local oceanic ecosystem remain to be determined.

Right now, combing remote sensing and statistic analysis, long-term time study is a valid means to investigate the variability of oceanic phenomenon (e.g. seasonal or interannual fluctuations and the spatial distributions) and provides insight into the marine biological processes (Peliz and Fiúza, 1999; Radiarta and Saitoh, 2008; Steinberg et al., 2001). The present work is conducted with the intention to give a refined but comprehensive description of the phytoplankton blooms southwest of Luzon Strait in winter conditions using 8-year satellite-derived data, historical ecological factors data and physical oceanographic parameters. In this paper, we focus on producing a relatively overall understanding of the

phytoplankton blooms southwest of Luzon Strait in winter, as well as determining the specific relationship between the biological feature and related physical processes in this region. The aim of this paper is to a) characterize the spatio-temporal patterns of the phytoplankton blooms southwest of Luzon Strait with statistic model and specify the high occurrence region of the phytoplankton blooms; b) investigate the controlling factors of the timing, intensity and location of the blooms by long-term time analysis; c) present a conceptional model to depict the mechanism of the winter blooms near Luzon Strait.

2. Study area, Data, and Methods

2.1 Study Area

The study area (Fig. 1B) is situated at 118.0 °E -121.0 °E, 17.0 °N -21.0 °N along part of Malina trench, which could reach to a depth about 5,000 m, but the average depth of the SCS is only about 1,500 m (Hayes and Lewis, 1984). The area is prevailed with northeast monsoon in winter and southwest monsoon in summer (Shaw and Chao, 1994), and the wind has influence on the local marine ecosystem (Tang et al., 1999).

2.2 Satellite-derived data

Sea surface Chlorophyll *a* (Chl *a*) concentration data were derived from the Sea-viewing Wide Field of view Sensor (SeaWiFS) launched in 1997 and MODIS Aqua launched in 1999. The data were obtained from the Distributed Active Archive Centre (DAAC), NASA, (http://oceancolor.gsfc.nasa.gov/). Monthly averaged Chl *a* images of MODIS Aqua in 2005 were processed for the study area, then individual scene was combined to compose seasonally mean chl *a* images using a cylindrical projection with the SeaWiFS Data Analysis System

(SeaDAS 5.3). SeaWiFS monthly 9-km resolution data from January 2000 to December 2007 were used for statistic analysis and long-term time study.

Sea surface temperature (SST) satellite-derived data were processed from MODIS Aqua. The seasonally composited MODIS SST images corresponding to the chl *a* images in 2005 were calculated in this study.

The vector winds data were retrieved from Quick Scatterometer (QuikSCAT), which was a polar orbiting satellite with an 1800 km wide measurement swath on the earth's surface (http://winds.jpl.nasa.gov/missions/quikscat/index.cfm). The data of 0.25 degree graded daily wind fields from 2000 to 2007 were processed and further analyzed to investigate the temporal and spatial variability in the study region.

2.2 Mixed-layer depth

Time series data of monthly mean mixed-layer depth for the study area from January 2000 to December 2006 were produced with the Giovanni online data system, developed and maintained by the NASA Goddard Earth Sciences (GES) Data and Information Services Center (DISC).

2.3 Ecological data sampling

Ecological factors data of oceanographic temperature, Dissolved Oxygen (DO), and nutrients (Phosphate (P), Silicate (Si), and Nitrate (N)) in the analysis were collected and processed at World Ocean Atlas 2005 (WOA05) from the National Oceanographic Data Center (NODC) hydrographic database. WOA05 based on in *situ* observations consisted of objectively analyzed monthly climatological fields of temperature (Locarnini et al., 2006), salinity (Antonov et al., 2006), DO, Apparent Oxygen Utilization, oxygen saturation (Garcia

et al., 2006a), and dissolved inorganic nutrients (Garcia et al., 2006b) at standard depth level (0, 10, 20, 30, 50, 75, 100, 125, 150, 200, 250, 300, 400 m,…,1500 m).

In this database, oceanographic temperature profile data were from bottle samples, Mechanical Bathythermograph (MBT), ship-deployed Conductivity-Temperature-Depth (CTD) package, Digital Bathythermograph (DBT), Expendable Bathythermograph (XBT), profiling float, moored and drifting buoys, gliders, and undulating oceanographic recorder (UOR) profiles (Locarnini et al., 2006). All of the quality-controlled O_2 (ml L^{-1}) data and the nutrient data used in the WOA05 were obtained by analysis of serial (discrete) water column samples (Garcia et al., 2006b). The O_2 values were analyzed by various modifications of the Winkler titration method using visual, amperometric, or photometric end-detections. The nutrient data calculated from the discrete water sample dataset, which consisted of 1 to 36 water samples were collected at various depths between the surface and the ocean bottom using Nansen or Niskin samplers (Garcia et al., 2006b).

2.4 Empirical Orthogonal Function Statistical analysis

The Empirical Orthogonal Function (EOF) analysis rooted in statistics aims at finding a new set of variables that captures most of the observed variance from the data through a linear combination of the original variables (Hardy, 1977; Kutzbach, 1967). It is referred to Principal Component Analysis (PCA) or eigenvector, which is initially applied to time series of meteorological data (Lorenz, 1956). The EOF method is also used to identify the dominant spatial and temporal patterns from series of remote sensing data (Emilie and Francis, 2009; Nezlin and McWilliams, 2003). In this study, the EOF approach is applied to analysis of remote sensing data from 2000 to 2007. The space patterns of Chl *a* revealed by the first and

second EOF mode show the spatial variability of Chl *a* in the study region. Spatial coefficients of the EOF modes represent the spatial extension and the dynamic importance of the processes in the study area (Navarro and Ruiz, 2006). The intensity of the phenomenon is directly related to the amplitude coefficient.

3. Results

3.1 Spatio-temporal characteristics of the phytoplankton blooms

The EOF analysis is used to identify the specified region of the phytoplankton bloom. The typical offshore pattern (Fig. 2A, B) and seasonal cycle (Fig. 2C) of Chl *a* concentration are showed in the southwest of Luzon Strait, and the eigenvector of the first EOF mode accounts for 60.1% of the total variance, the second mode only 11.6%. Spatial patterns show patch of strong positive signal of Chl *a* concentration centering at 119.0°E,19.0°N about 2.58×10^4 km^2 off the coast of northwest Philippines (i.e. the phytoplankton blooms always occur at this place) (Fig. 2A, B), while the Chl *a* concentration exhibits a decreasing gradient (relatively weaker signal) around the patch. The lowest Chl *a* concentration with the weakest signal occurs at the entrance of Luzon Strait. The quantified seasonal variability is reflected by the temporal amplitude (Fig. 2C) associated with the spatial pattern of the first mode (Fig. 2A). The positive signals with prominent peak of Chl *a* concentration generally appear in winter per year. Moreover, the time series of monthly averaged SeaWiFS data of the study area also show the same seasonality with highest concentration (0.43 mg m^{-3}) in winter and lowest in summer (0.08 mg m^{-3}) (Fig. 5A).

Further analysis of annual variation of the phytoplankton blooms were depicted by

177 seasonally averaged MODIS images of Chl *a* concentration and SST (Fig. 3A, B) in 2005. A
178 patch of phytoplankton community southwest of Luzon Strait in winter (Dec.-Feb.) was
179 reflected by higher Chl *a* concentrations (> 0.3 mg m^{-3}) than other three seasons (Fig. 3A).
180 Meanwhile, this bloom centering at 118.5°E,19.7°N was located in the bloom region which
181 was calculated by EOF method (Fig. 2A). However, no remarkable differences of SST were
182 evidenced in winter in the study area (Fig. 3B.1).

183 **3.2 Surface wind conditions**

184 Influenced by the Asian monsoon, the regional wind condition alternated the wind
185 intensity and direction in different seasons (Fig. 3C). In winter (Dec.-Feb.), strong northeast
186 winds about 16 m s^{-1} appeared at the entrance of Luzon Strait along the coastline of northwest
187 tip of Philippine (Fig. 3C.1). During summer (Jun.-Aug.), the wind near Luzon Strait was
188 obviously weaker than wind intensity of the region above Luzon Strait around Taiwan (Fig.
189 3C.3), with the opposite direction to it of winter. Perhaps spring (Mar.-May.) and autumn
190 (Sep.-Nov.) were the transitional periods in the monsoon system, and the wind conditions in
191 these two seasons were relatively moderate with changing directions (Fig. 3C.2, C.3). Fig 5B
192 show the variations of spatial averaged wind curl in the study area for the period of
193 2000-2007. The velocity sticks illustrate prevailing northeast wind about 12 m s^{-1} in winter
194 and southwest about 4 m s^{-1} in summer time.

195 **3.2 Mixed-layer depth reaching to about 60 m**

196 The spatial mean time series of the mixed-layer depth (Fig. 5C) in the study region show
197 that an apparent seasonal variability coincided with Chl *a* concentration fluctuation (Fig. 5A)
198 and local spatial averaged wind curl (Fig. 5B). From the linear regression analysis, a high

correlation coefficient (r=0.83) at the 95% confidence level is evidenced between chl *a* concentration data of the study area and mixed-layer depth of the same region. The mixed-layer is deepening all the time in autumn, to reach to a maximum about 60 m in winter every year. From spring, the mixed-layer depth is begin to shallow and reaches to a minimum approximate 12 m in summer time.

3.3 Vertical variation of temperature, DO and nutrients in January 2005

Horizontal distributions of temperature (Fig. 4A-F) in January 2005 showed that a striking cold temperature core (< 19.0 ℃) was appeared at 50 m depth in the study area (Fig. 4D), and the feature was more obvious in deeper sea water (75 m, 100 m) (Fig. 4E, F). At the depth of 0 m (Fig. 4A), 20m (Fig. 4B) and 30m (Fig. 4C), there were no signals of the cold water mass, and temperature was gradually increasing from northwest to southeast in the study area. Fig. 6 illustrated the vertical distributions of DO, N, P, Si from surface to a depth of 250 m averaged from 10 stations (Fig. 4D) which were located in the cold water core. The DO concentration in the upper 50 m ranged from 5.13 mg L^{-1} to 4.86 mg L^{-1}. However, it varied from 4.52 mg L^{-1} to 2.95 mg L^{-1} below 50 m to the depth of 250 m (Fig. 6A). The profile of N (Fig. 6B) displayed a narrow fluctuation between 0.82 μM and 1.96 μM in the top 50 m. Below the depth of 50 m, the concentration of N rapidly increased with depth, reaching to a peak value of 29.30 μM at the depth of 250 m. The vertical profiles of P and Si concentrations showed similar trend to that of N. The concentration of P (Fig. 6C, D) was low from sea surface to the depth of 50 m and maintained little changes range from 0.43 μM to 0.57 μM; a prominent increasing trend with depth was showed between the depths of 50 m and 250 m. The Si profile (Fig. 6D) also displayed little variation above the depth of 50 m and

221 reached to a maximum of 59.10 μM at the depth of 250 m.

222

223 **4. Discussion**

224 **4.1** The high occurrence region of the phytoplankton blooms limited by nutrients

225 The results reveal the high occurrence area of winter phytoplankton blooms centering at
226 119.0°E,19.0°N about 2.58×10^4 km^2 by statistic model (Fig. 2). The biological productivity is
227 high in this region during winter off the tips of northwest Philippines. Previous studies have
228 been shown that all those blooms are located in the high occurrence bloom region defined in
229 this study. High pigment concentration southwest of Luzon Strait was centering at 118.5°E,
230 19.0°N in December 1979 (Tang et al., 1999). The blooms also appeared in January and
231 February 1983 centered at 119.0°E, 20.0°N and in February 1985 centered at 120.0°E, 19.5°N
232 (Tang et al., 1999). In December 2003, the blooms center was at 118.5°E, 19.5°N and the
233 highest chl *a* concentration reached to approximately 2.0 mg m^{-3} (Peñaflor et al., 2007).

234 Phytoplankton production in the ocean is normally limited by nutrients availability and
235 solar radiation (Dwivedi, 2008; Siegel et al., 2007; Tang et al., 2004a). The study area is
236 located in the high solar irradiated latitude of the vicinity of Luzon Strait in the SCS which is
237 the relatively oligoltrophic tropical-subtropical ocean (Tang et al., 2004b; Tang et al., 1999).
238 Averaged winter SST about 24.3 °C is good for the growth of phytoplankton (Peñaflor et al.,
239 2007). Moreover, monthly mean photosynthetically active radiation (PAR) observed in winter
240 around the study area is at high value (Chen et al., 2006). Therefore, winter phytoplankton
241 blooms which always occur within the area about 2.58×10^4 km^2 in the southwest of Luzon
242 Strait are majorly controlled by nutrient availability rather than radiation conditions.

4.2 Subsurface upwelling and mixed-layer depth deepening during blooms

The typical upwelling region is associated with high productivity due to upwelled nutrient-rich water from deep to sea surface (Labiosal and Arrigo, 2003; Tang et al., 2004b; Wilkerson et al., 2006), and the upwelling is reflected by cold sea surface water, low DO concentration as well as sea level anomaly (Collins et al., 2003; Martin and Villanoy, 2008; Shaw et al., 1996; Tang et al., 2002). However, southwest of Luzon Strait appears to have significant differences from other classic upwelling regions. The upwelling located in the study region can be identified by its anomalously subsurface phenomenon including cold sea temperature (< 19.0 ℃) (Fig. 4), low DO (Fig. 6A)and high nutrients (Fig. 6B-D) observed at the depth of 50 m only in winter time. The variation of DO concentration was within ±0.14 mg L^{-1} in the upper 50 m depth and dramatically decreased from 4.52 mg L^{-1} to 2.95 mg L^{-1} below 50 m to the depth of 250 m (Fig. 6A). Dissolved inorganic nutrients (N, P, and Si) reached to the limits from deeper water only to subsurface at the depth of 50 m (Fig 6B-D).This is why this atypical upwelling is unable to be detected by remote sensing or field study from the sea surface parameters in every winter. In addition, low heat content is observed in this subsurface upwelling area (Udarbe-Walker and Villanoy, 2001). An elongated band of low sea level in the study region in wintertime also supports the upwelling exist (Martin and Villanoy, 2008).But the high productivity can not believe to occur solely in association with the subsurface upwelling which unlikely pumps nutrients into the euphotic zone to support the growth of phytoplankton.

4.3 Mechanism of the offshore winter phytoplankton bloom

4.3.1 wind-related physical and biological processes

Wind events in the sea play an important role in establishing the physical and biological processes (Botsford et al., 2006; Tang et al., 2003). The results demonstrate that the upwelling in the southwest of Luzon Strait is a subsurface phenomenon depended on local bottom topography and offshore Ekman pumping associated northeast monsoonal winds. The research region with low sea surface level in winter (Martin and Villanoy, 2008) is above part of Malina trench with the depth of about 5,000 m; the bottom topography at this place is complex with a steep slope (Fig. 1B). The sea level anomaly is related with the subsurface upwelling events, because the topographic steering of the winds moves surface water away and offshore Ekman transport induces the upwelling. However, cold upwelled waters with low DO and high nutrients are exposed at subsurface layer (Fig. 4). Phytoplankton growth in the study area is regulated primarily by nutrient availability. The subsurface upwelling just permits the transportation of nutrients to the low layer, which is impossible to support the growth of phytoplankton in the euphotic zone of the upper layer. Therefore, the key to understanding the formation of the winter blooms lies in elucidation of the possible mechanism of the nutrients supply to the upper layer.

Time series of mixed-layer depth with local and synoptic wind forcing indicate that winds in winter are much stronger than in summer, the surface mixed-layer in the study area deepens more than 60 m during winter and becomes as shallow as 10m to 20m in summertime in response to the monsoonal winds (Fig. 5A, C). The strong winds during winter promote evaporative cooling to drive convective mixing and make the upper ocean in a turbulent situation. The tendency of turbulence to diffuse into the adjoining non-turbulent layer leads to the erosion of the underlying stratification of the thermocline, namely entrainment

phenomenon, thus increasing the mixed-layer thickness (Backhaus et al., 2003; Labiosal and Arrigo, 2003; Strang and Fernando, 2001). The entrainment brings nutrients which support the growth of phytoplankton from the low layer to the upper layer. The influences of entrainment also enhance the effects on mixing the nutrients and phytoplankton in the upper layer (Madhupratap et al., 1996). The well-mixed nutrients of N, P, and Si in the upper layer demonstrate the existence of entrainment (Fig. 6B-D). The concentrations of N, P, and Si change slightly in the upper 50 m; dramatic increasing is evidenced below this layer.

4.3.2 Conceptional model of the winter blooms formation

The schematic pictures of winter and summer conditions (Fig.7) illustrate the mechanism of the offshore winter phytoplankton bloom. Strong wind stress during the winter northeast monsoon (Fig. 7A) results in Ekman transport, which induces the subsurface upwelling near the slope. Nutrients from the bottom or deep sea are transported to low layer by upwelled waters. Then turbulence intensifies mixing generated by stronger local wind string near the surface, which increases entrainment of water from below. During this process, mixed layer is deepening below the euphtotic zone. More nutrients are continuously being offered to maintain the growth of phytoplankton, because turbulence mixes nutrients brought by subsurface upwelling from low layer towards to the upper layer beyond the euphotic layer. At this time, the study area turns to be a high biological productive region. On the contrary, the wind direction is southwest in summer and weaker. It seems unlikely that the wind can induce subsurface upwelling owing to the local bottom topography and strong stratification in this area (Fig. 7B). Without the availability of nutrients from low layer, phytoplankton biomass in the study area was low in this season.

5. Conclusions

The region near Luzon Strait is oligotrophic in general, but it displays some unique features in wintertime. The present study reveals that phytoplankton in the southwest of Luzon Strait exhibits a repeated winter bloom appearing within the high occurrence area about 2.58×10^4 km^2 southwest of Luzon Strait off the coast of Philippines, and the bloom is caused by sufficient nutrients associated with subsurface upwelling and upper mixed-layer entrainment.

Both the biological and physical processes in the study region have great relationship with winds. Nutrients are upwelled into the low layer by subsurface upwelling induced by positive Ekman pumping, subsequently entrained into the upper layer to support the growth of phytoplankton while turbulence is generated by local wind stirring. The present observations and explanations may provide insight on the contribution of different physical forcing to biological processes in the ocean and better understanding the interaction between physical and biological processes.

Acknowledgements

This work was jointly supported by (1) National Natural Sciences Foundation of China (40976091, 40811140533) and Guangdong Natural Science Foundation (8351030101000002); (2) Key Project of Knowledge Innovation Program, Chinese Academy of Sciences (KZCX2-YW-226; LYQY200701), (3) The CAS/SAFEA International Partnership Program for Creative Research Teams (KZCX2-YW-T001). The authors greatly appreciate data

providers. We extend thank Dr. Xinfeng Zhang of Shanghai Ocean University and Fei Wang of South China Sea Institute of Oceanology, Chinese Academy of Sciences for their valuable help and comments on this study.

References

Antonov, J.I., R. A. , Locarnini, T.P., Boyer, A.V., Mishonov and Garcia, H.E., 2006. World Ocean Atlas 2005, 2: Salinity. S. Levitus, Ed. NOAA Atlas NESDIS 62, U.S. Government Printing Office, Washington, D.C., 182 pp. .

Backhaus, J.O. et al., 2003. Convection and primary production in winter. Mar. Ecol. Prog. Ser., 251: 1-14.

Botsford, L.W., Lawrence, C.A., Dever, E.P., Hastings, A. and Largier, J., 2006. Effects of variable winds on biological productivity on continental shelves in coastal upwelling systems. Deep Sea Res. Part II, 53(25-26): 3116-3140.

Chen, C.C., Shiah, F.K., Chung, S.W. and Liu, K.K., 2006. Winter phytoplankton blooms in the shallow mixed layer of the South China Sea enhanced by upwelling. J. Mar. Sys., 59(1-2): 97-110.

Collins, C.A., Pennington, J.T., Castro, C.G., Rago, T.A. and Chavez, F.P., 2003. The California Current system off Monterey, California: physical and biological coupling. Deep Sea Research Part II, 50(14-16): 2389-2404.

Dwivedi, R.M.e.a., 2008. Formation of algal bloom in the northern Arabian Sea deep waters during January-March: a study using pooled in situ and satellite data. Int. J. Remote Sens., 29(15): 4537-4551.

Emilie, T.-K. and Francis, M., 2009. Patterns of variability of sea surface chlorophyll in the Mozambique Channel: A quantitative approach. J. Mar. Sys., 77(1-2): 77-88.

Farris, A. and Wimbush, M., 1996. Wind-induced Kuroshio Intrusion into the South China Sea. J. Oceanogr., 52: 771-784.

375 Garcia, H.E., Locarnini, R.A., Boyer, T.P. and Antonov, J.I., 2006b. World Ocean Atlas 2005, 4:
376 Nutrients (phosphate, nitrate, silicate). S. Levitus, Ed. NOAA Atlas NESDIS 64, U.S.
377 Government Printing Office, Washington, D.C., 396 pp. .
378 Garcia, H.E., R. A. , Locarnini, T.P., Boyer and Antonov, J.I., 2006a. World Ocean Atlas 2005, 3:
379 Dissolved Oxygen, Apparent Oxygen Utilization, and Oxygen Saturation. S. Levitus, Ed.
380 NOAA Atlas NESDIS 63, U.S. Government Printing Office, Washington, D.C., 342 pp. .
381 Hardy, D.M., 1977. Empirical eigenvector analysis of vector observations. Geophys. Res. Letters, 4:
382 319-320.
383 Hayes, D.E. and Lewis, S.D., 1984. A geophysical study of the Manila trench, Luzon, Philippines. 1.
384 Crustal structure, gravity and regional tectonic evolution. J. Geophys. Res., 89(B11):
385 9171-9195
386 Kutzbach, J.E., 1967. Empirical eigenvectors of sea-level pressure, surface temperature and
387 precipitation complexes over North America. J. Appl. Meteorol., 6: 791-802.
388 Labiosal, R.G. and Arrigo, K.R., 2003. The interplay between upwelling and deep convective mixing in
389 determining the seasonal phytoplankton dynamics in the Gulf of Aqaba: Evidence from
390 SeaWiFS and MODIS. Limnol. Oceanogr., 48(6): 2355-23368.
391 Liu, A.K. and Hsu, M.K., 2003. Nonlinear internal wave study in the South China Sea using SAR. Int. J.
392 Remote Sensing, 25: 1-5.
393 Locarnini, R.A., A. V., Mishonov, J.I., Antonov, T.P., Boyr and Garcia, H.E., 2006. World Ocean Atlas
394 2005, 1: Temperature. S. Levitus, Ed. NOAA Atlas NESDIS 61, U.S. Government Printing
395 Office, Washington, D.C., 182 pp. .
396 Lorenz, E.N., 1956. Empirical Orthogonal Functions and Statistical Weather Prediction, Scientific

Report 1, Statistical Forecasting Project, Mass. Inst. Tech., Cambridge, Mass. (Defense Doc. Center No. 110268). 49 pp.

Madhupratap, M. et al., 1996. Mechanism of the biological response to winter cooling in the northeastern Arabian Sea. Nature, 384(6609): 549-552.

Martin, M.C. and Villanoy, C.L., 2008. Sea Surface Variability of Upwelling Area Northwest of Luzon, Philippines, Dynamic Planet. Springer Berlin Heidelberg, pp. 84-87.

Navarro, G. and Ruiz, J., 2006. Spatial and temporal variability of phytoplankton in the Gulf of Cáiz through remote sensing images. Deep Sea Res. Part II, 53(11-13): 1241-1260.

Nezlin, N.P. and McWilliams, J.C., 2003. Satellite data, Empirical Orthogonal Functions, and the 1997–1998 El Niño off California. Remote Sens. Environ., 84(2): 234-254.

Peñaflor, E.L., Villanoy, C.L., Liu, C.-T. and David, L.T., 2007. Detection of monsoonal phytoplankton blooms in Luzon Strait with MODIS data. Remote Sens. Environ., 109(4): 443-450.

Peliz, A.J. and Fiúza, A.F.G., 1999. Temporal and spatial variability of CZCS-derived phytoplankton pigment concentrations o. the western Iberian Peninsula. Int. J. Remote Sensing, 20(7): 1363± 1403.

Radiarta, I.N. and Saitoh, S.-I., 2008. Satellite-derived measurements of spatial and temporal chlorophyll-a variability in Funka Bay, southwestern Hokkaido, Japan. Estuarine Coastal Shelf Sci., 79: 400-408.

Shaw, P.-T., Chao, S.-Y., Liu, K.-K., Pai, S.-C. and Liu, C.-T., 1996. Winter upwelling off Luzon in the northeastern South China Sea J. Geophys. Res., 101: 16435-16448.

Shaw, P.T. and Chao, S.Y., 1994. Surface cirulation in the South China Sea. Deep Sea Res. Part I, 41: 1663-1683

419 Siegel, H., Ohde, T., Gerth, M., Lavik, G. and Leipe, T., 2007. Identification of coccolithophore blooms
420 in the SE Atlantic Ocean off Namibia by satellites and in-situ methods. Cont. Shelf Res., 27(2):
421 258-274.
422 Steinberg, D.K. et al., 2001. Overview of the US JGOFS Bermuda Atlantic Time-series Study (BATS):
423 a decade-scale look at ocean biology and biogeochemistry. Deep Sea Res. Part II, 48(8-9):
424 1405-1447.
425 Strang, E.J. and Fernando, H.J.S., 2001. Entrainment and mixing in stratified shear flows. J. Fluid
426 Mech., 428: 349-386.
427 Tang, D.L., Kawamura, H. and Luis, A.J., 2002. Short-term variability of phytoplankton blooms
428 associated with a cold eddy in the northwestern Arabian Sea. Remote Sens. Environ., 81(1):
429 82-89.
430 Tang, D.L., Kawamura, H., Dien, T.V. and Lee, M.A., 2004a. Offshore phytoplankton biomass increase
431 and its oceanographic causes in the South China Sea. Mar. Ecol. Prog. Ser., 268: 31-41.
432 Tang, D.L., Kawamura, H., Doan-Nhu, H. and Takahashi, W., 2004b. Remote sensing oceanography of
433 a harmful algal bloom off the coast of southeastern Vietnam. J. Geophys. Res.-Oceans, 109.
434 Tang, D.L., Kawamura, H., Lee, M.-A. and Van Dien, T., 2003. Seasonal and spatial distribution of
435 chlorophyll-a concentrations and water conditions in the Gulf of Tonkin, South China Sea.
436 Remote Sens. Environ., 85(4): 475-483.
437 Tang, D.L., Ni, I.-H. and Kester, D.R., 1999. Remote sensing observations of winter phytoplankton
438 blooms southwest of the Luzon Strait in the South China Sea. Mar. Ecol. Prog. Ser., 191:
439 43-51.
440 Udarbe-Walker, M.J.B. and Villanoy, C.L., 2001. Structure of potential upwelling areas in the

Philippines. Deep Sea Res. Part I, 48(2001): 1499-1518.

Wang, B. et al., 2009. Multi-scale climate variability of the South China Sea monsoon: A review. Dyn. Atmos. Oceans, 47: 15-37.

Wilkerson, F.P., Lassiter, A.M., Dugdale, R.C., Marchi, A. and Hogue, V.E., 2006. The phytoplankton bloom response to wind events and upwelled nutrients during the CoOP WEST study. Deep Sea Res. Part I, 53: 3023–3048.

Wu, C.-R. and Chiang, T.-L., 2007. Mesocale eddies in the northern South China Sea Deep Sea Res. Part II, 54: 1575-1588.

Wyrtki, K., 1961. Physical Oceanography of the Southeast Asia Waters NAGA *Report*, 2: 1-195.

Figure Captions

Fig. 1 A. Location of study area; B. Bathymetry map of study area (black bold line box) in SCS. The white dash indicated the Malina Trench.

Fig. 2 A. Spatial pattern of the first EOF on Sea Surface Chl *a* data. Percentage of variance is 60.1%. The dotted cross shows the extent of phytoplankton bloom; B. Spatial pattern of the second EOF mode accounts for 11.6% of the total variance. The arrow points the center of the bloom; C. Time series of the amplitude of the first EOF mode.

Fig. 3 Seasonal images of 2005. A. MODIS-derived Chl *a* in (A.1) winter, (A.2) spring, (A.3) summer, (A.4) autumn. The ellipse and arrow indicate the offshore bloom phenomena; B. MODIS-derived SST. The ellipse in (B.1) shows SST without any abnormal state in the bloom region in winter; C. QuickScat wind. The small arrows indicate wind directions, and the color indicates wind speed. The large arrow and ellipse in (C.1) point out the bloom area experienced strong wind in winter.

Fig. 4 Sea temperature distribution at 0 m, 20 m, 30 m ,50 m, 75 m and 100 m depth in January, 2005.The ellipses in D, E and F indicate the subsurface upwelling phenomenon; The sampling stations in D for DO and nutrients analysis.

Fig. 5 Temporal variations of the study area for A. SeaWiFS-derived Chl *a*; B. wind; C. mixed-layer depth. W: winter; S: summer.

Fig. 6 Ecological data sampling profiles averaged from the 10 stations (shown as Fig. 6D) in January, 2005. A. DO profile; B. N profile; C. P profile; and D. profile of Si from surface to the depth of 250 m.

Fig. 7 Schematic of phytoplankton bloom in A. winter and B. summer.

Figure 1.

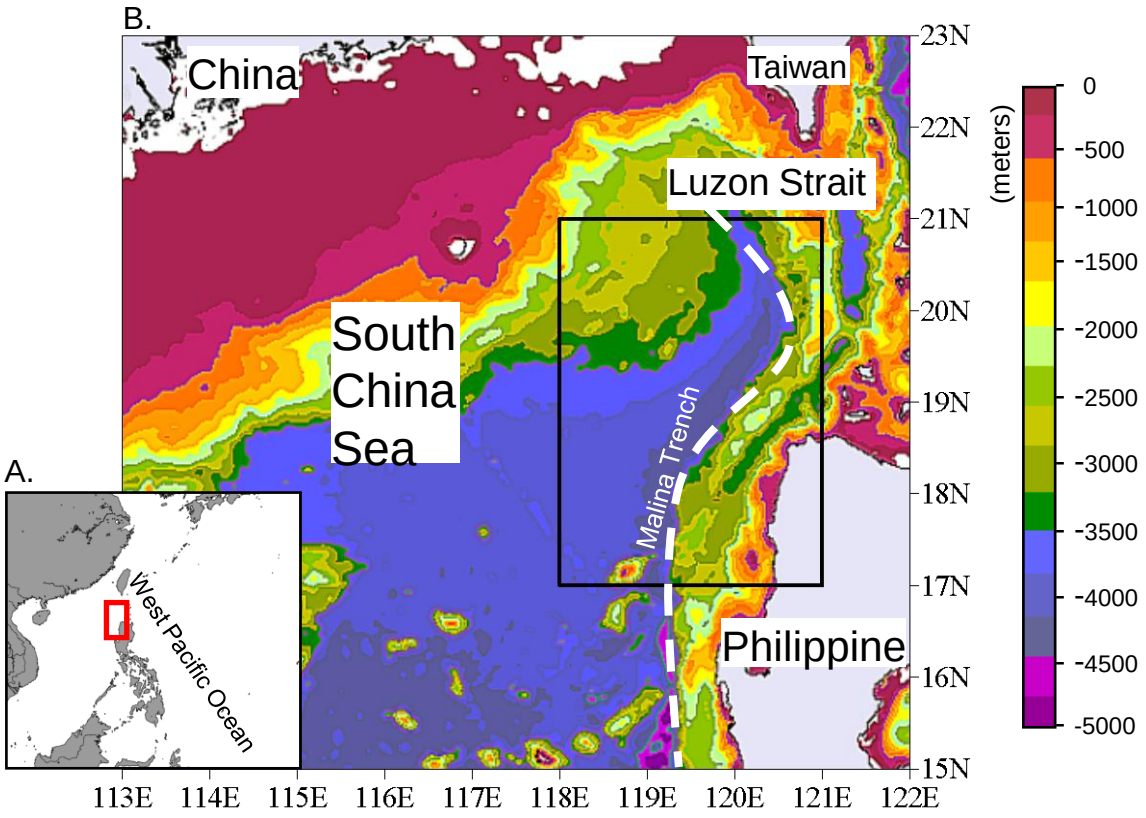
B.
China
Taiwan
Luzon Strait
South China Sea
Malina Trench
Philippine
A.
West Pacific Ocean
23N
22N
21N
20N
19N
18N
17N
16N
15N
113E
114E
115E
116E
117E
118E
119E
120E
121E
122E
(meters)
0
-500
-1000
-1500
-2000
-2500
-3000
-3500
-4000
-4500
-5000

Figure 2.

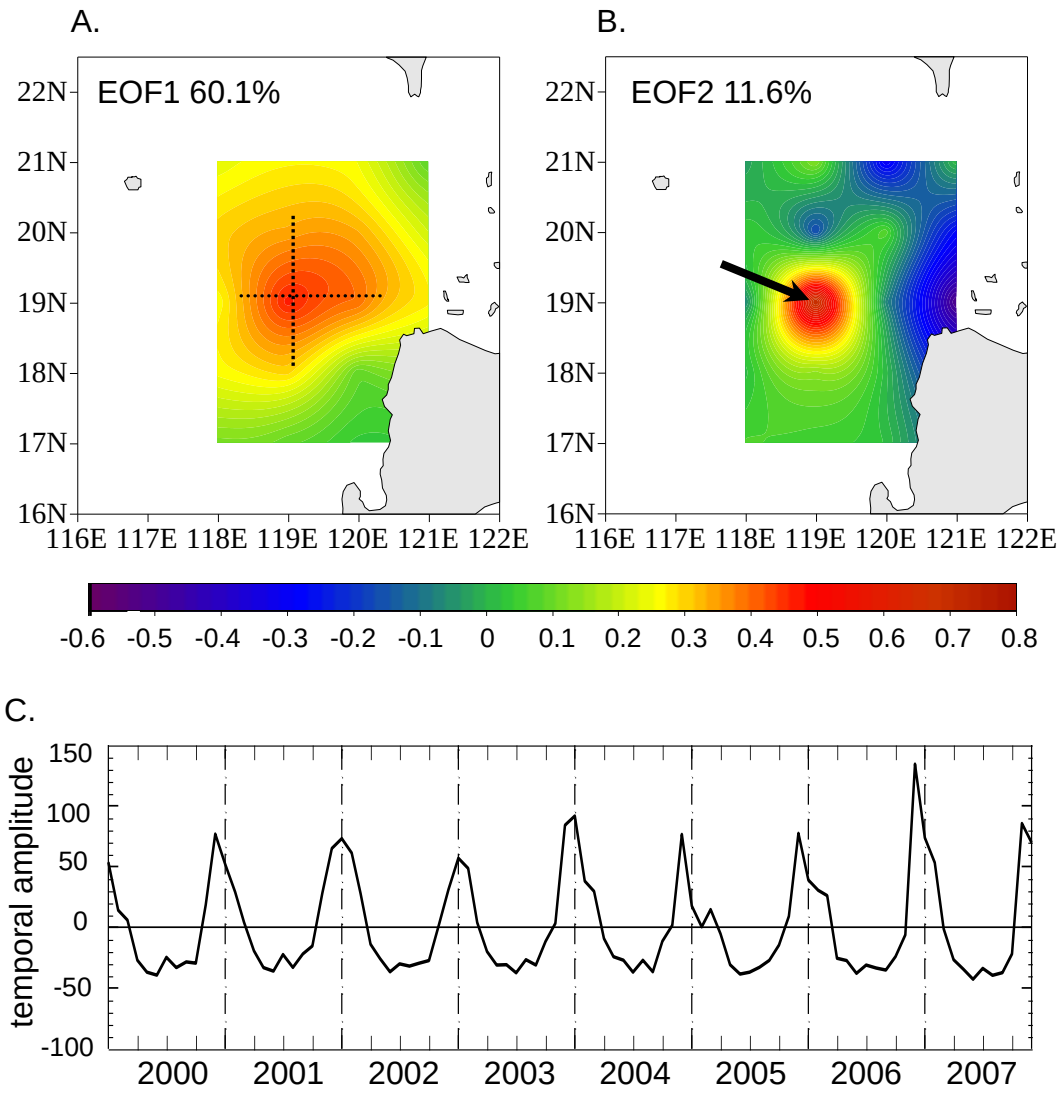
A.
EOF1 60.1%
B.
EOF2 11.6%
22N
21N
20N
19N
18N
17N
16N
116E 117E 118E 119E 120E 121E 122E
-0.6 -0.5 -0.4 -0.3 -0.2 -0.1 0 0.1 0.2 0.3 0.4 0.5 0.6 0.7 0.8
C.
temporal amplitude
150
100
50
0
-50
-100
2000 2001 2002 2003 2004 2005 2006 2007

Figure 3.

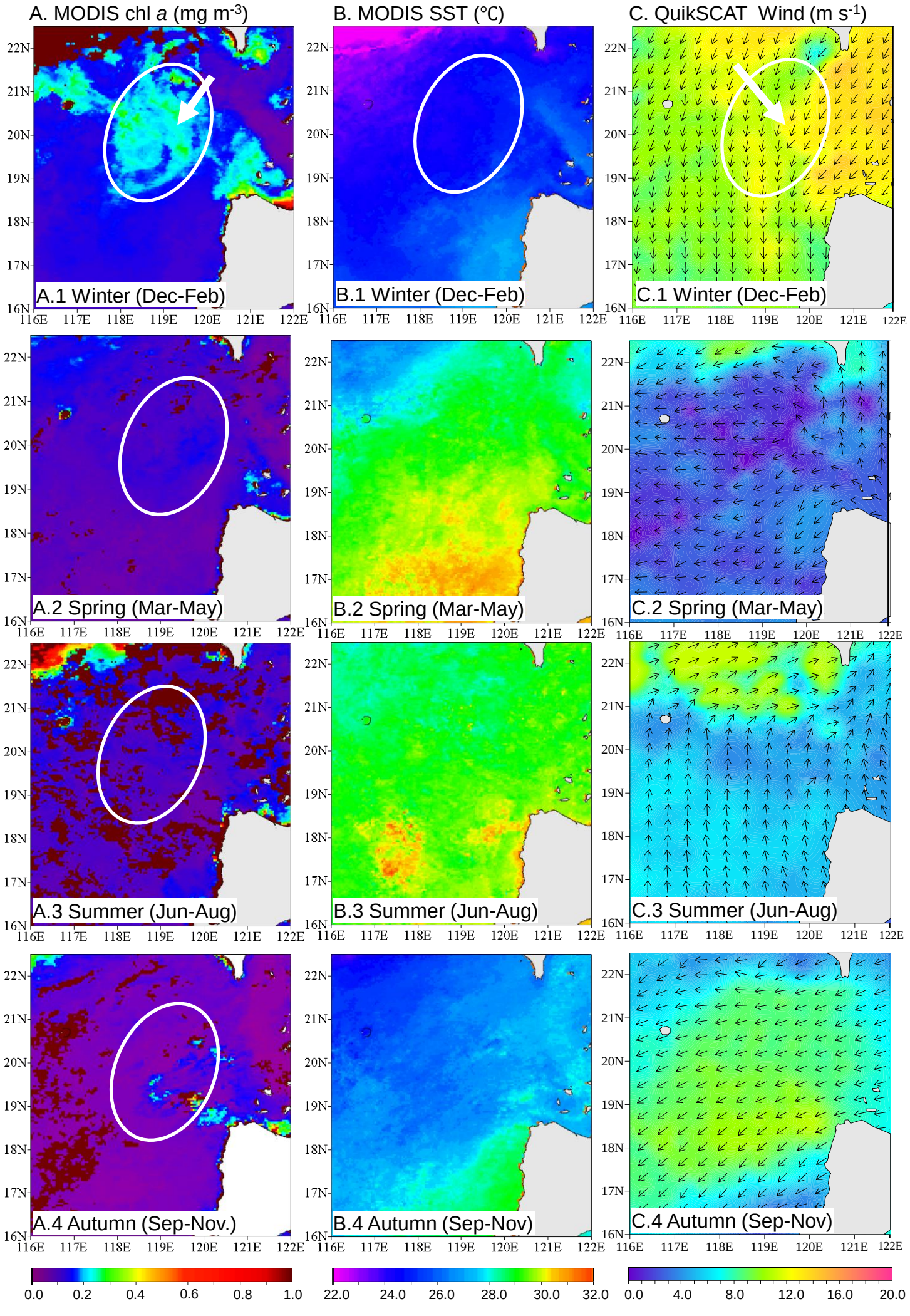
A. MODIS chl a (mg m-3)
B. MODIS SST (℃)
C. QuikSCAT Wind (m s-1)
A.1 Winter (Dec-Feb)
B.1 Winter (Dec-Feb)
C.1 Winter (Dec-Feb)
A.2 Spring (Mar-May)
B.2 Spring (Mar-May)
C.2 Spring (Mar-May)
A.3 Summer (Jun-Aug)
B.3 Summer (Jun-Aug)
C.3 Summer (Jun-Aug)
A.4 Autumn (Sep-Nov.)
B.4 Autumn (Sep-Nov)
C.4 Autumn (Sep-Nov)
22N
21N
20N
19N
18N
17N
16N
116E
117E
118E
119E
120E
121E
122E
0.0
0.2
0.4
0.6
0.8
1.0
22.0
24.0
26.0
28.0
30.0
32.0
0.0
4.0
8.0
12.0
16.0
20.0

Figure 4.

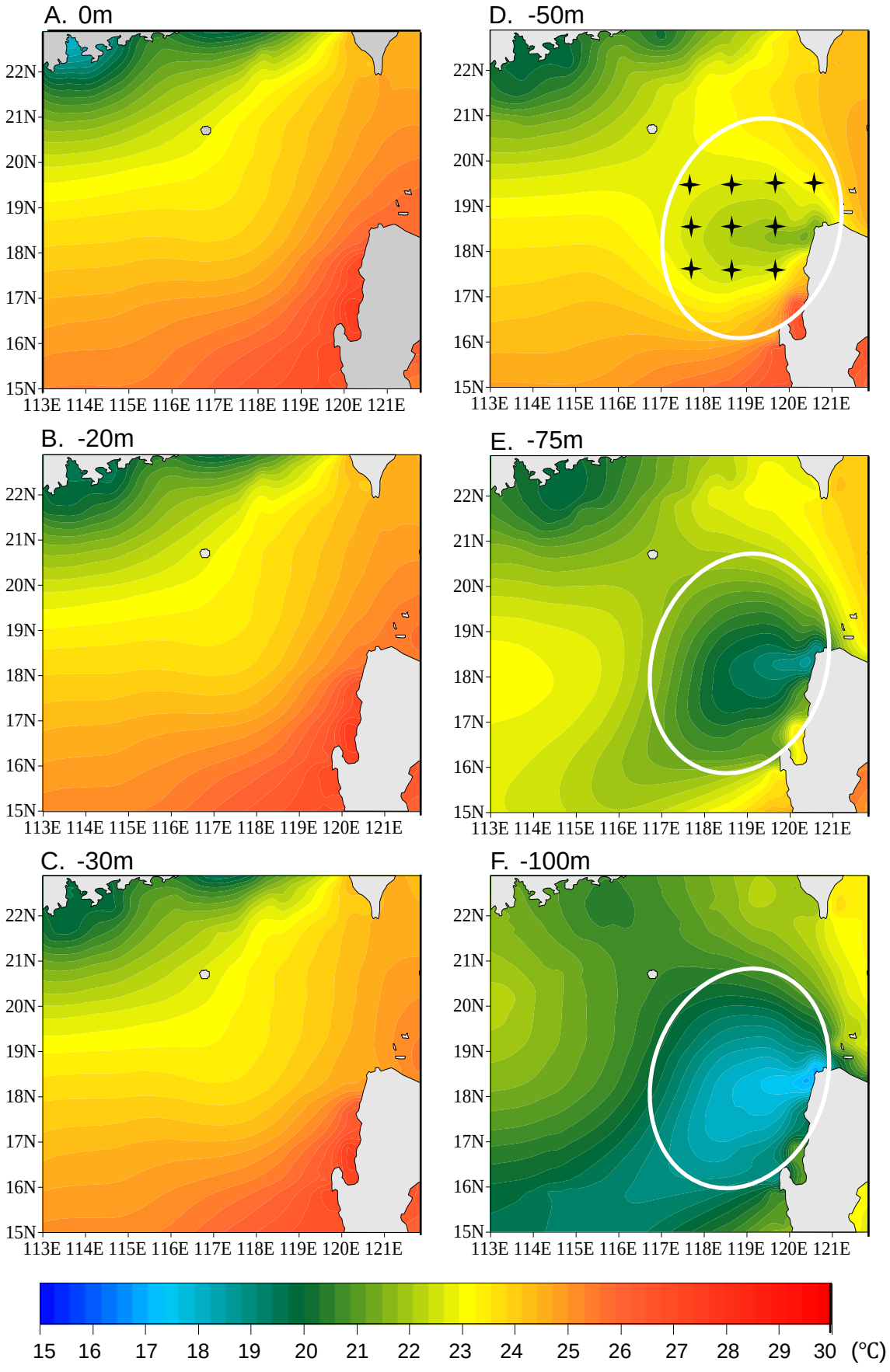
A. 0m
D. -50m
B. -20m
E. -75m
C. -30m
F. -100m
22N
21N
20N
19N
18N
17N
16N
15N
113E 114E 115E 116E 117E 118E 119E 120E 121E
15 16 17 18 19 20 21 22 23 24 25 26 27 28 29 30 (℃)

Figure 5.

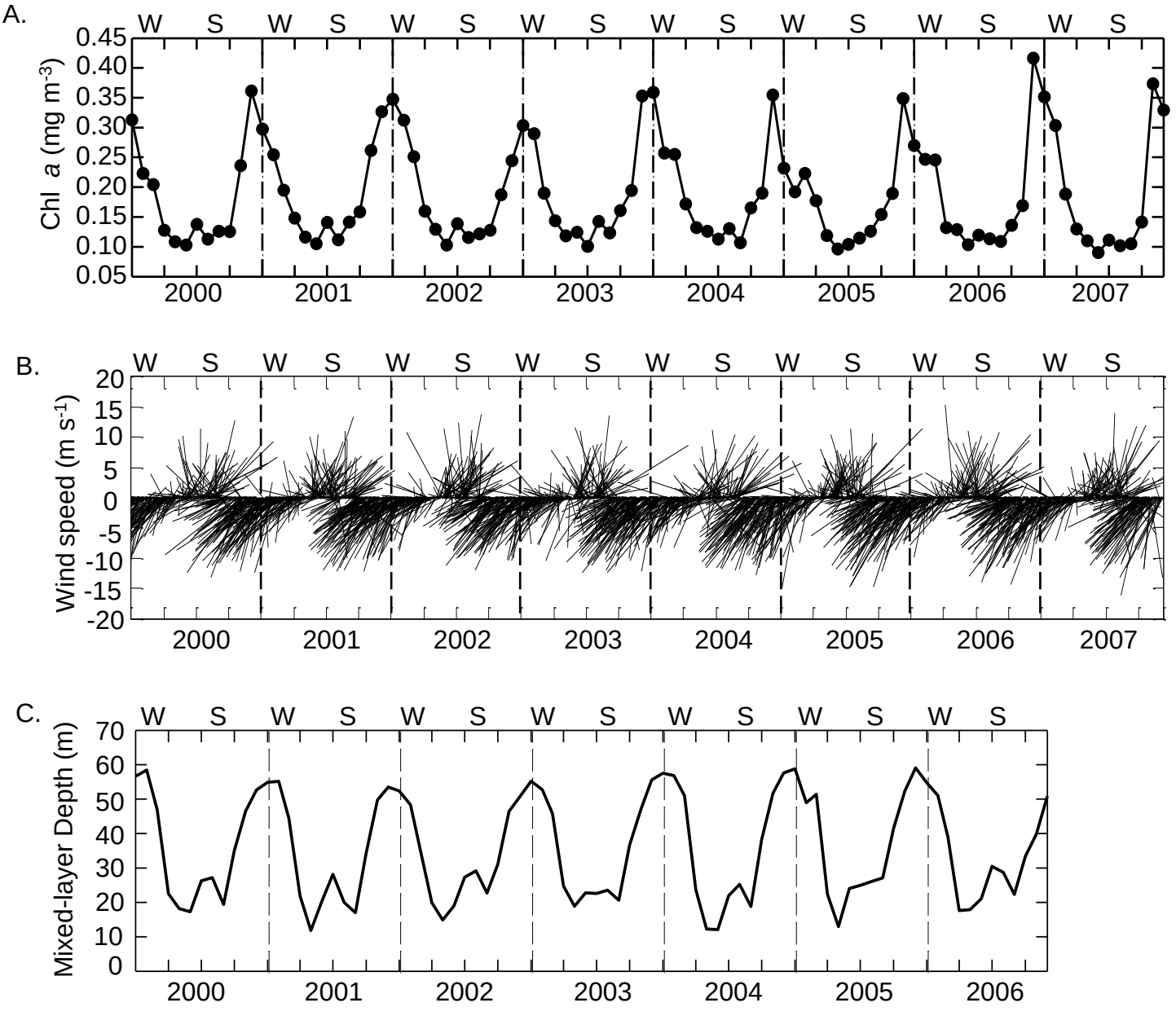
A.
W S W S W S W S W S W S W S W S W S
0.45
0.40
0.35
0.30
0.25
0.20
0.15
0.10
0.05
Chl a (mg m-3)
2000 2001 2002 2003 2004 2005 2006 2007
B.
W S W S W S W S W S W S W S W S W S
20
15
10
5
0
-5
-10
-15
-20
Wind speed (m s-1)
2000 2001 2002 2003 2004 2005 2006 2007
C.
W S W S W S W S W S W S W S W S
70
60
50
40
30
20
10
0
Mixed-layer Depth (m)
2000 2001 2002 2003 2004 2005 2006

Figure 6.

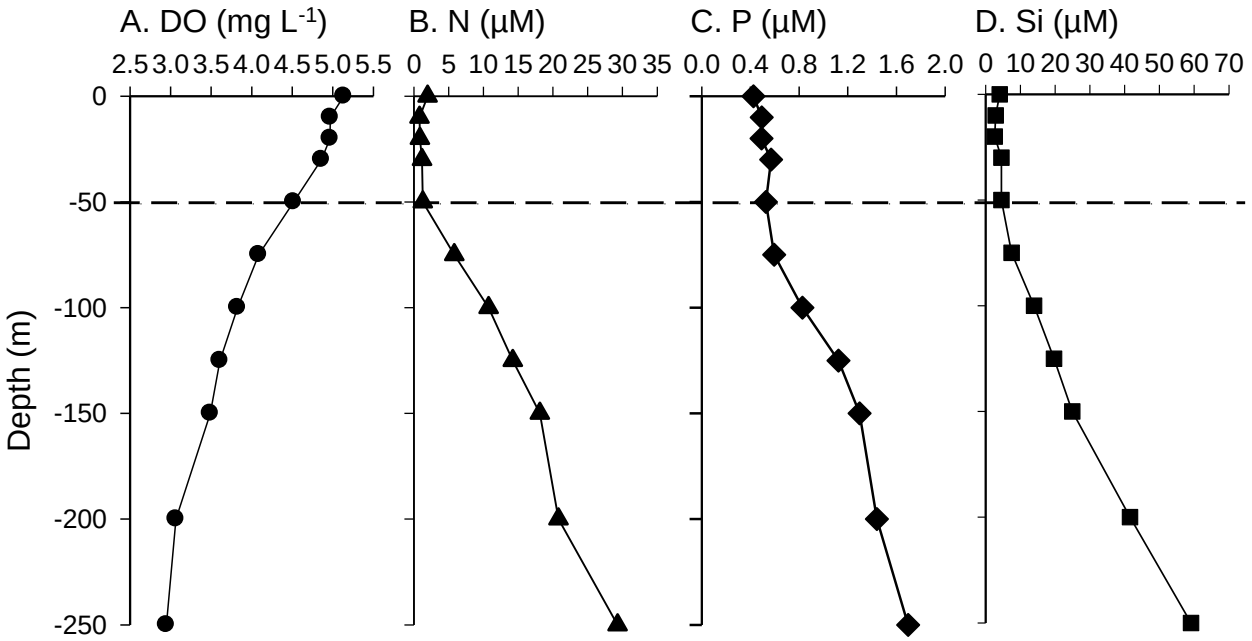
A. DO (mg L-1)
2.5 3.0 3.5 4.0 4.5 5.0 5.5
B. N (µM)
0 5 10 15 20 25 30 35
C. P (µM)
0.0 0.4 0.8 1.2 1.6 2.0
D. Si (µM)
0 10 20 30 40 50 60 70
Depth (m)
0
-50
-100
-150
-200
-250

Figure 7.

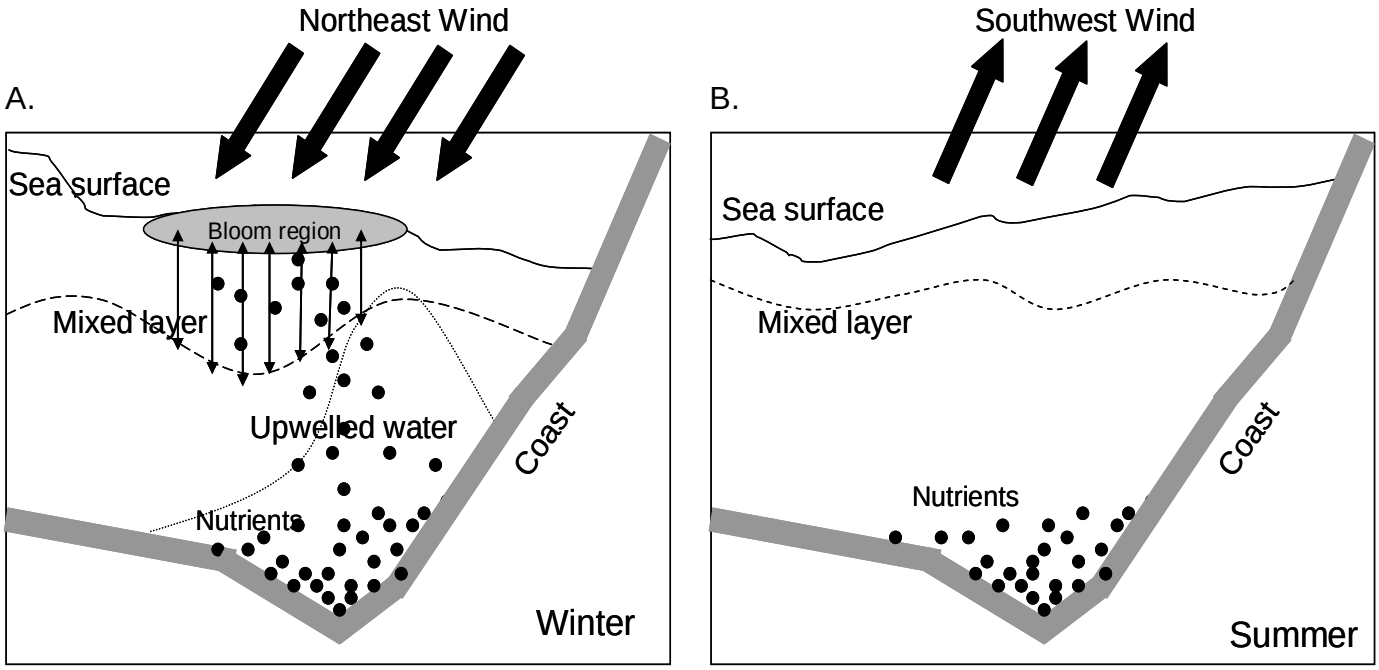
A.
Northeast Wind
Sea surface
Bloom region
Mixed layer
Upwelled water
Nutrients
Coast
Winter
B.
Southwest Wind
Sea surface
Mixed layer
Nutrients
Coast
Summer